

BROOKHAVEN NATIONAL LABORATORY

September 1989

Received by OSTI
BNL-43385
NOV 06 1989

DEFORMED PROXIMITY POTENTIAL FOR HEAVY ION REACTIONS

BNL--43385

DE90 002295

A.J. Baltz

Physics Department
Brookhaven National Laboratory
Upton, New York 11973

ABSTRACT

The proximity potential is discussed for the inelastic scattering of a spherical nucleus on a deformed nucleus or the mutual interaction of two deformed nuclei. It is shown that the proximity potential is, in general, geometrically more correct than the usual centerline prescription used in inelastic scattering analyses. For the cases where the proximity potential is inadequate a folding model approach is advocated. Techniques to facilitate the coupled channels analysis are presented.

*An invited talk presented
at
Sixth Nordic Meeting on Nuclear Physics
Kopervik, Norway
August 10-15, 1989

This manuscript has been authored under contract number DE-AC02-76-CH00016 with the U.S. Department of Energy. Accordingly, the U.S. Government retains a non-exclusive, royalty-free license to publish or reproduce the published form of this contribution, or allow others to do so, for U.S. Government purposes.

MASTER

DISTRIBUTION OF THIS DOCUMENT IS UNLIMITED

1. INTRODUCTION AND BACKGROUND

In heavy ion reactions low lying collective states of both projectile and target can be strongly excited by Coulomb excitation over a broad range of projectile energies, and by the nuclear interaction when the reaction occurs above the Coulomb barrier. The discussion here will be confined to the nuclear excitation of inelastic degrees of freedom in nuclei during heavy ion collisions. In particular, the case will be treated when one or both of the nuclei are statically deformed. Since the interaction is strong, with multi-step processes the norm. reaction calculations must be carried out in the framework of large sets of coupled Schrödinger equations. This aspect of the problem will be discussed in Section 4. We will first concentrate on the interaction that causes the inelastic transitions, namely a deformed optical potential.

The usual treatment of the deformed optical model involves a potential which is a function of the distance between the nuclear surfaces along a line connecting the nuclear centers (Fig. 1) For a spherical nucleus interacting with a deformed nucleus, such a potential obviously depends on the distance between their centers as well as the orientation of the deformed nucleus. Randrup and Vaagen¹ pointed out that a more correct proximity treatment of the potential involves two geometrical corrections to this center-line prescription:

1. The point of least separation distance, at which the proximity formulation is applied, is in general not on the line connecting the two centers²; and
2. the local curvature, which determines the strength of attraction, varies along the surface of a deformed nucleus.

The original proximity interaction derived by Blocki *et al.*³ was based on consideration of the energy density of the ion-ion system. An alternative way of thinking of the proximity potential is as an approximation to the folding model. Since the folding model has its greatest validity in the tail of the potential and it is just this region that is probed by the peripheral inelastic scattering reactions, we will use the folding model as a standard for comparison and development of the proximity model.

For simplicity, first consider spherical nuclei; the generalization to deformed nuclei will be straightforward. We take a single folding approach in which a nucleon-projectile optical

potential is folded over the density of the target. (This is equivalent to a folding of the densities of the two nuclei with a delta-function nucleon-nucleon interaction.) For gently curved surfaces, one may consider the interaction energy per unit area of two parallel surfaces at separation s .

The essential approximation of the proximity treatment is to replace the spherical surfaces with paraboloids of the same Gaussian curvature, thus allowing the integration to be done in a universal way. One obtains an ion-ion potential expressed in terms of the principal radii of curvature of the two surfaces (R_{ij}) times a "slab on slab" function of the separation distance, ϵ_0 , which is based on the density distributions of the two slabs.³

$$V(s) = 2\pi \sqrt{\frac{R_{1x}R_{2x}}{R_{1x} + R_{2x}}} \sqrt{\frac{R_{1y}R_{2y}}{R_{1y} + R_{2y}}} \epsilon_0(s). \quad (1.1)$$

Brink⁴ pointed out that if the densities of both nuclei are of Woods-Saxon form with the same diffusivity, a , then in the proximity approximation the folded potential becomes

$$V_P^F(R) = 2\pi V_P^0 \rho_T^0 \frac{R_T R_P}{R_T + R_P} \int_{R - R_T - R_P}^{\infty} \frac{s ds}{\exp(s/a) - 1}. \quad (1.2)$$

This form provides a convenient universal ion-ion potential with which we can investigate the deformed proximity potential. Of course other ion-ion potentials correspond to the folding of other effective nuclear densities. For example, the Woods-Saxon potential is obtained in the proximity approximation from the folding of two densities peaked at the nuclear surfaces.⁵

2. THE PROXIMITY POTENTIAL FOR A SPHERICAL NUCLEUS INTERACTING WITH A DEFORMED NUCLEUS

One generalizes from the spherical to the deformed proximity potential by finding the minimum separation distance between the two nuclei and then taking the operative curvature of the deformed nucleus at that point on the surface closest to the spherical nucleus⁵ (Fig. 1). This is the approach originally taken by Randrup and Vaagen in their analytical but approximate treatment.¹

To attain quantitative adequacy, our approach is semi-numerical: while we obtain analytical expressions for the radii of curvature, we use a computer search to find the point on the deformed nucleus closest to the spherical nucleus. The potential for a given

orientation is then expressed in terms of the radius of curvature of the spherical nucleus and in terms of the two principal radii of curvature of the deformed nucleus at the appropriate point.

Expressions for the principal radii of curvature along a deformed surface, $R_1(\theta)$ and $R_2(\theta)$, are given in Ref. 5. Generation of the deformed proximity potential in terms of the spherical radius of curvature R_P and the two deformed radii of curvature $R_1(\theta)$ and $R_2(\theta)$ is then straightforward. One takes the geometric mean of the two perpendicular curvature factors to obtain

$$V_{P1}(R, \theta) = 2\pi \sqrt{\frac{R_1(\theta) R_P}{R_1(\theta) + R_P}} \sqrt{\frac{R_2(\theta) R_P}{R_2(\theta) + R_P}} \epsilon_0(s). \quad (2.1)$$

where $\epsilon_0(s)$ is the ‘‘slab on slab’’ function dependent on the separation distance, s , and the density profile of the two nuclei.

Up to now we have only really treated the real part of the optical potential. One does not expect the folding picture to have much validity for the imaginary potential. We will assume, however, that the geometrical picture of the deformed proximity potential can be taken over to the imaginary potential in conjunction with a Woods-Saxon or other empirical potential for the slab on slab radial form. As we pointed out, one can show in the proximity picture that the Woods-Saxon potential form can be seen to arise out of a surface-surface folding. This picture does not seem geometrically unreasonable for the generation of a heavy ion imaginary potential. Adopting a one term proximity potential treatment of the deformed imaginary potential we obtain

$$W_P(R, \theta) = W(s) \sqrt{\frac{R_1(\theta) R_P}{R_1(\theta) + R_P}} \sqrt{\frac{R_2(\theta) R_P}{R_2(\theta) + R_P}} \left(\frac{R_T + R_P}{R_P R_T} \right) \quad (2.2)$$

where $W(s)$ is any empirical potential form and R_T is the spherical radius corresponding to the average radius of the deformed nucleus.

This potential form might also be utilized for the real potential if one did not want to abandon empirical Woods-Saxon potentials, but nevertheless wanted to provide a geometrically more correct treatment of deformation.

For comparison we calculate the angular momentum components of the angle dependent optical potentials for both folded, proximity, and centerline potentials

$$V_L(R) = \int d\Omega Y_L^0(\Omega) V(R, \theta). \quad (2.3)$$

To investigate various aspects of the deformed proximity potential we previously investigated a case for which data exist and for which a coupled channels analysis⁶ had been performed: 72 MeV $^{16}\text{O} + ^{152}\text{Sm}$. Geometrically, this is a typical case, a light heavy ion projectile on a more massive deformed target.

Since the V_0 component is ultimately fit to elastic data, the ratio of computed components to the $L = 0$ component must be reliably calculated for reliable extraction of multipole moments. We found that the ratios of components for $L = 2, 4, 6$ to the $L = 0$ component were in good agreement for the proximity and folding models.⁵

However, the crucial point of this whole development is how the proximity model treatment differs from the centerline prescription when higher multipole components are extracted. We have plotted in Figure 2 the ratios of angular momentum components to the real monopole potential using the centerline prescription and the Woods-Saxon proximity potential of Eq. (2.2). Assuming the Woods-Saxon proximity potential has the more correct relative geometry for the given deformation lengths ($\beta_2 R_N^2 = 1.65$, $\beta_4 R_N^4 = .29$), we find that V_4/V_0 and V_6/V_0 are significantly overpredicted in the centerline prescription for the $\beta_4 R_N^4$ value of .29, implying a true value somewhat larger. In fact there is a discrepancy between this value obtained in Kim's heavy ion analysis and the values of $\beta_4 R_N^4 = .52$ and .53 from electron scattering and Coulomb excitation respectively. If we keep $\beta_2 R_N^2$ at 1.65 and set $\beta_4 R_N^4$ to .52 then we obtain ratios for the Woods-Saxon proximity model which are very close to the ratios of the centerline prescription in Figure 2 probed by Kim's analysis.

To further test these observations coupled channels calculations have been performed for this case using the coupled channels code QUICC.⁷ In Figure 3 the solid line is a repetition of Kim's original calculation for the 4^+ angular distribution, using the centerline prescription and $\beta_2 R_N^2 = 1.65$, $\beta_4 R_N^4 = .29$, which fits the data. The dotted line is a Woods-Saxon proximity potential calculation with the same parameters. The dashed line is a Woods-Saxon proximity potential calculation with $\beta_4 R_N^4 = .52$ and all other parameters the same. Clearly the proximity potential calculation with $\beta_4 R_N^4 = .52$ corresponds better to the centerline calculation of $\beta_4 R_N^4 = .29$ and thus to the data. Using the more correct proximity prescription has caused the discrepancy with the electron scattering and Coulomb excitation results to disappear.

3. FORM FACTORS FOR THE INTERACTION BETWEEN TWO DEFORMED NUCLEI

Bayman has derived proximity potential form factors for mutual excitation of deformed nuclei, including simultaneous direct excitation of both ions.^{8,5} A coordinate system is chosen in which the z -axis runs through the centers of the two interacting nuclei (Fig. 4). The relative position and orientations of the two nuclei then can be completely described by four variables: the distance between the centers, R , the inclination of each of the nuclei from the z -axis, θ_1 and θ_2 , and the rotation angle of the second nucleus about the z -axis relative to the first, ϕ . As Bayman points out, the proximity potential implies a torque about centerline (z -axis) which is absent in the centerline prescription.

The technical details of how the shortest distance between the two deformed nuclei in this configuration is obtained have been given in Ref. 8. A proximity potential can then be defined in terms of two principal radii of curvature of each of the nuclei evaluated at the mutual points on the surface closest to the other nucleus. The expressions are complicated, but amenable to a computer. A proximity potential is obtained as a function of R , θ_1 , θ_2 and ϕ .

By integrating over the three angular variables, form factors can be obtained of various angular momentum character for each value of the distance R between the nuclear centers. However Bayman's form factor expressions can be applied to any potential function of R , θ_1 , θ_2 and ϕ to obtain the appropriate transition form factor, e.g. to the folding model or the centerline prescription (even though it is independent of ϕ). I have made a small extension of Bayman's computer code PROX in order to be able to make a sample comparison of the three models. The form factor I consider is the one for simultaneous inelastic excitation of the 2^+ level in ^{24}Mg and the 4^+ level in ^{154}Sm , the case in which Bayman compared DWBA calculation for the proximity and centerline potentials. Optical model parameters and deformations have been taken from Ref. 8.

Figure (5) shows a comparison of the three form factors for the Woods-Saxon density folding or Brink potential case. For angular momentum transfer 6, the proximity potential is in good agreement with the folding model and the center line prescription is not. For the lower angular momentum transfers of 4 and 2 the situation is less clear cut. The shapes

and magnitudes of the proximity potential are certainly in much better agreement with the folding model than the centerline potential is. However the quantitative agreement is less than ideal. In fact, for a simpler case in which the ^{154}Sm target is not excited, but the strongly deformed ^{28}Si projectile is directly excited to the 4^+ state, the form factor calculated in the proximity model is about half the magnitude of that calculated in the folding model.

If one takes the approach that the proximity potential should reproduce the deformed geometry of the folding model, then it seems clear that for quantitative analysis of heavy ion reactions one should simply adopt the folding geometry when the proximity model is inadequate. This is not to diminish the importance of the simplicity and physical insight available from the proximity potential. However, the constant improvements of computing makes routine evaluations of even all orientations of two deformed nuclei for the folding model quite feasible.

4. THE COUPLED CHANNELS PROBLEM

It has been pointed out that for mutual excitation of two deformed nuclei the total number of coupled channels that must be included for each scattering partial wave becomes very large even for relatively low lying states being excited in both nuclei. For example, inclusion of rotational levels up to maximum I for each nucleus leads to a total number of channels

$$N = \frac{(I^2 + 2I + 2)(I + 2)^2}{8}$$

for each partial wave.⁸ Thus including excitation of the 0^+ , 2^+ , 4^+ , and 6^+ states of each ground state band would lead to 400 channels; including the 8^+ also would make it 1025 channels.

Such a calculation is within the realm of current possibility as far as the number of channels. A heavy ion coupled channels calculation has been performed for a spherical nucleus on a deformed target which required 441 channels: $^{208}\text{Pb} + ^{238}\text{U} (0^+, 2^+, \dots, 40^+)$.⁹ This is a quantum mechanical calculation with a complex deformed optical potential. Fig. (6) shows the distribution of cross section into final states in the grazing region for a 1400 MeV projectile. The transition from the "picket fence" pattern characteristic of Coulomb

excitation at the forwardmost angle to the smooth distribution of the final states characteristic of the onset of the complex nuclear interaction at more backward angles is evident. This calculation made use of the centerline potential, and should be viewed as illustrative. A proximity potential calculation would not significantly increase the time or difficulty of the calculation. Such a calculation could easily be performed if data existed of a quality sufficient to determine the optical parameters and the higher multipole deformations.

Some discussion should be made on how such a large calculation can be carried out in a reasonable amount of computer time. Several techniques facilitate the computation:

(1) Solution of the coupled equations is iterative. A set of coupled first order equations equivalent to the usual second-order coupled Schrödinger equations is solved. The wave function solutions in each channel ($r u_i(r) = \chi_i(r)$) are written in terms of radially varying coefficients, $C_i(r)$, $C_i^+(r)$, of the regular and outgoing, $f_i(r)$, $h_i^+(r)$, parts of the homogeneous (uncoupled) wave function solutions:

$$\chi_i(r) = C_i(r) f_i(r) - C_i^+(r) h_i^+(r) . \quad (4.1)$$

One then immediately obtains from the second order coupled Schrödinger equations two sets of coupled first order equations in $C_i(r)$ and $C_i^+(r)$:

$$\begin{aligned} \frac{d}{dr} C_i(r) = & \frac{1}{k_i} [h_i^+(r) \sum_j V_{ij}(r) f_j(r) C_j(r) \\ & - h_i^+(r) \sum_j V_{ij}(r) h_j^+(r) C_j^+(r)] \end{aligned} \quad (4.2a)$$

$$\begin{aligned} \frac{d}{dr} C_i^+(r) = & \frac{1}{k_i} [f_i(r) \sum_j V_{ij}(r) f_j(r) C_j(r) \\ & - f_i(r) \sum_j V_{ij}(r) h_j^+(r) C_j^+(r)] \end{aligned} \quad (4.2b)$$

The first equation is integrated inward, beginning by ignoring the second term on the right-hand side and using the asymptotic initial condition of only incoming flux in the elastic channel ($C_i(\infty) = -2i\delta_{io}$) for the first term. Next, the second equation may be integrated outward beginning with the approximate but very adequate physical boundary condition that $C_i^+(r_0) = 0$ for some small r_0 . The process is then iterated to convergence.

(2) The Coulomb excitation is solved quantum mechanically, but in a way that takes numerical advantage of its semiclassical character. The variation on the method which I

have developed for the Coulomb excitation region is to break the products of homogeneous wavefunction on the right-hand side into rapidly oscillating and smoothly varying parts. The rapidly oscillating parts may then be discarded in all orders of the iteration, allowing a large step size for the solution in the long-range part.⁷ However, in the nuclear interaction and turning point region the equations are solved exactly.

(3) Only a relatively few partial waves are calculated. For the case discussed 10,000 partial waves were included in the Legendre polynomial sum for the final cross sections. However, only 65 were actually calculated. The other scattering amplitudes were then obtained by interpolation for the partial wave sum.¹⁰

To reiterate, apart from the partial wave interpolation, the strengths of the method used for this problem are that it is iterative and that it allows solutions of the equations in the long range Coulomb excitation region with a crude step size. Both of these features seem necessary to make the present problem tractable, as will be shown in the following. Solution of the equations was carried out to 400 fm. With the mesh size used in the turning point region (0.01 fm) a brute force second order Schrödinger equation approach would have required nearly 40,000 radial mesh points. By the technique of keeping only the smoothly varying parts of the effective long range coupling in the first order equations, the number of mesh points used was limited to about 500. The number of iterations needed to solve the 441 coupled equations for each partial wave never exceeded six to achieve an accuracy of one part in 10,000. In contrast, the brute force method would have required 441 independent sets of solutions of the set of 441 coupled equations followed by solving the appropriate set of 441 simultaneous equations for the scattering amplitudes.¹¹ The fast methods used allowed a full angular distribution to be calculated in about ten hours on the Cray 2 at MFE Livermore.

5. CONCLUSIONS

Low energy heavy ion reactions provide a rich opportunity for probing the mutual interactions of deformed nuclear surfaces. Strong interference effects between the nuclear interaction and Coulomb excitation make excited state angular distributions very sensitive to deformation parameters. This has been seen in extraction of the β_4 parameter from the 4^+ cross section in the $^{16}\text{O} + ^{154}\text{Sm}$. β_6 and higher moments could be similarly

analyzed from cross sections to higher final states. The technical problems of evaluating the appropriate deformed ion-ion potentials and performing the large scale coupled channels calculations are well in hand. What is now needed is more resolved final state data and application of the various coupling and transition schemes to coupled channels calculations.

ACKNOWLEDGMENTS

This research was supported under contract number DE-AC02-76-CH0016 with the U.S. Department of Energy.

REFERENCES

1. J. Randrup and J.S. Vaagen, Phys. Lett. 77B, 170 (1978).
2. D.L. Hendrie, Phys. Rev. Lett. 31, 478 (1973).
3. J. Blocki, J. Randrup, W.J. Swiatecki, and C.F. Tsang, Ann. of Phys. 105, 427 (1977).
4. D.M. Brink, *Proc. European Conference on Nuclear Physics with Heavy Ions*, Caen, France (1976), J. de Phys. 37, C5 (1976).
5. A.J. Baltz and B.F. Bayman, Phys. Rev. C26, 1969 (1982).
6. B.-T. Kim, Phys. Lett. 80, 353 (1979).
7. A.J. Baltz, Phys. Rev. C25, 240 (1982).
8. B.F. Bayman, Phys. Rev. C34, 1346 (1986).
9. A.J. Baltz, Phys. Rev. C38, 1674 (1988).
10. M. Rhoades-Brown, M.H. Macfarlane and S.C. Pieper, Phys. Rev. C21, 2417 (1980); 21, 2436 (1980).
11. T. Tamura, Oak Ridge National Laboratory Report # ORNL-4152, 1967 (unpublished).

DISCLAIMER

This report was prepared as an account of work sponsored by an agency of the United States Government. Neither the United States Government nor any agency thereof, nor any of their employees, makes any warranty, express or implied, or assumes any legal liability or responsibility for the accuracy, completeness, or usefulness of any information, apparatus, product, or process disclosed, or represents that its use would not infringe privately owned rights. Reference herein to any specific commercial product, process, or service by trade name, trademark, manufacturer, or otherwise does not necessarily constitute or imply its endorsement, recommendation, or favoring by the United States Government or any agency thereof. The views and opinions of authors expressed herein do not necessarily state or reflect those of the United States Government or any agency thereof.

Figure Captions

- Fig. 1: Coordinate system for a deformed optical potential including a volume element for folding.
- Fig. 2: Comparison of ratios of $L = 2, 4, 6$ components of the Woods-Saxon potential of Ref. 6 to the $L = 0$ component using the centerline prescription and the proximity prescription.
- Fig. 3: Comparison of $^{152}\text{Sm} (^{16}\text{O}, ^{16}\text{O}') ^{152}\text{Sm}(4^+)$ angular distribution. The value of the Woods-Saxon proximity real and imaginary potential depths have been reduced by 6% to correspond to the $L = 0$ potential strength of the conventional Woods-Saxon potential.
- Fig. 4: Coordinates frame for the interaction of two deformed nuclei.
- Fig. 5: Form factors for the simultaneous transition to the 2^+ state in ^{24}Mg and the 4^+ state in ^{154}Sm from the ground state of each. Curves are ratios of transition potentials to the spherical potential for the folding model (solid line), the proximity potential (dashed line), and the centerline potential (dot-dashed line). Total angular momentum L transferred is 6 (a), 4 (b) and 2 (c).
- Fig. 6: Cross sections ratios to Rutherford scattering at 84° (full circles), 88° (open circles), 92° (crosses), 96° (triangles), 100° (full squares), and 104° (open squares).

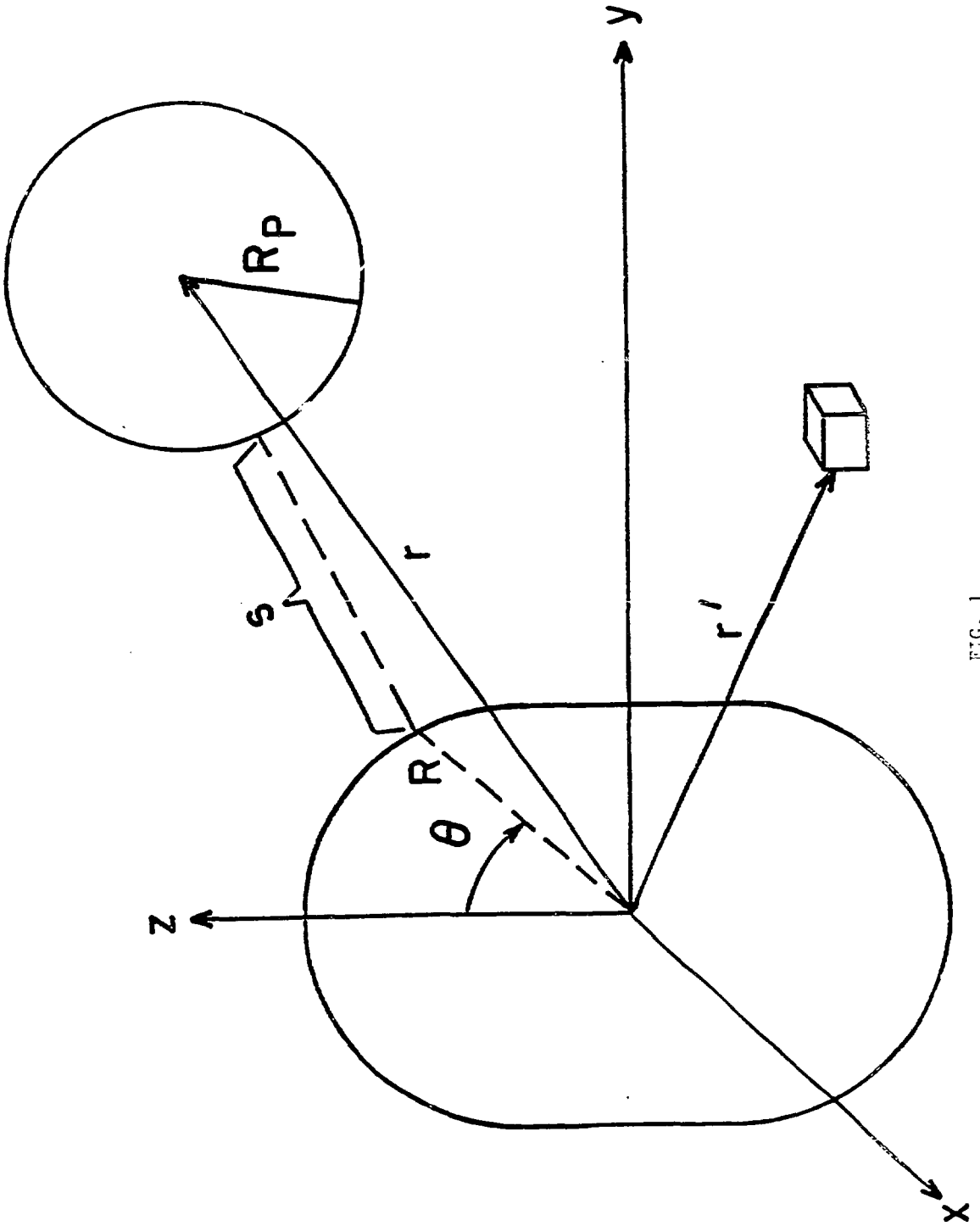


FIG. 1

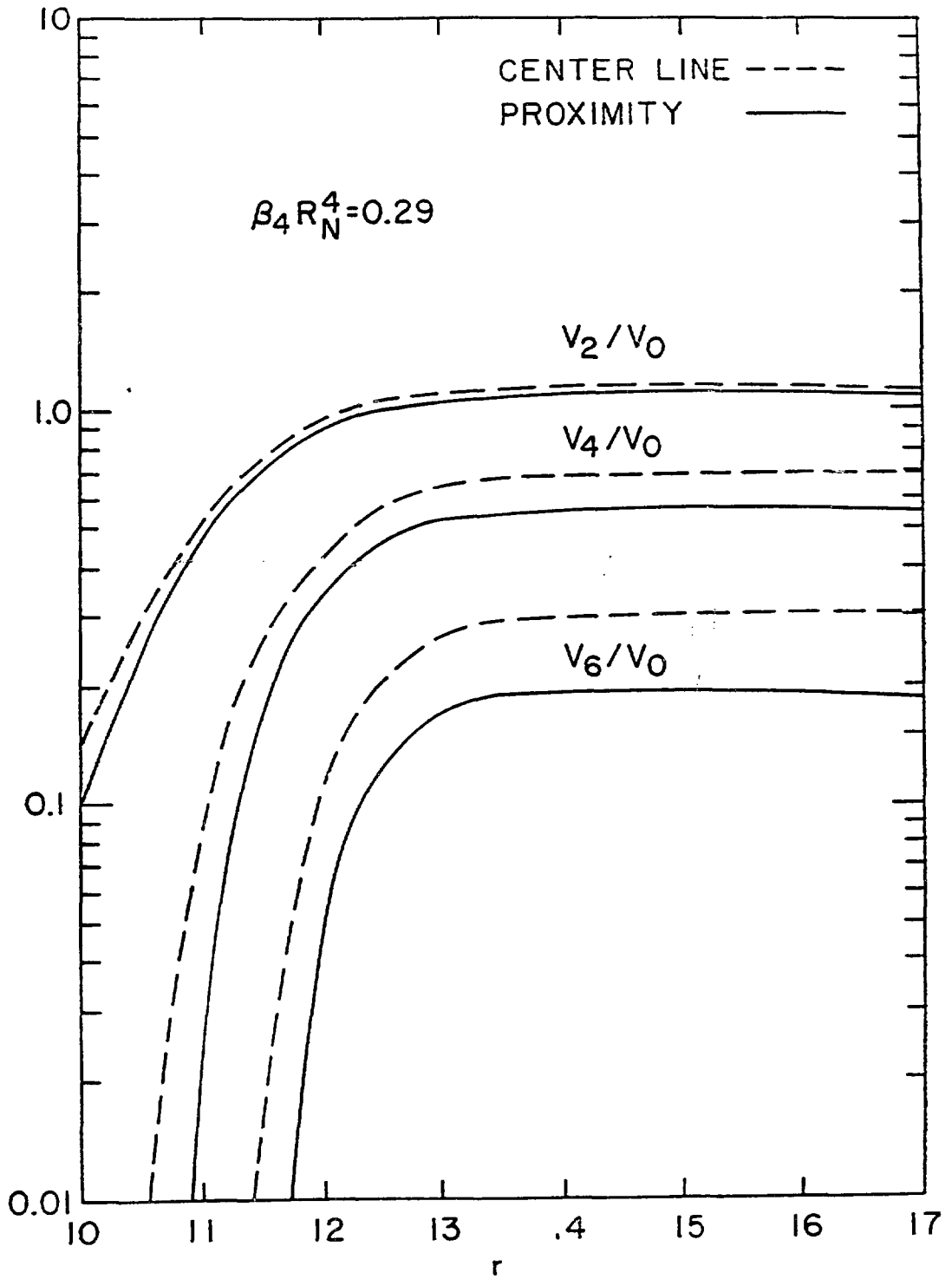


FIG. 2

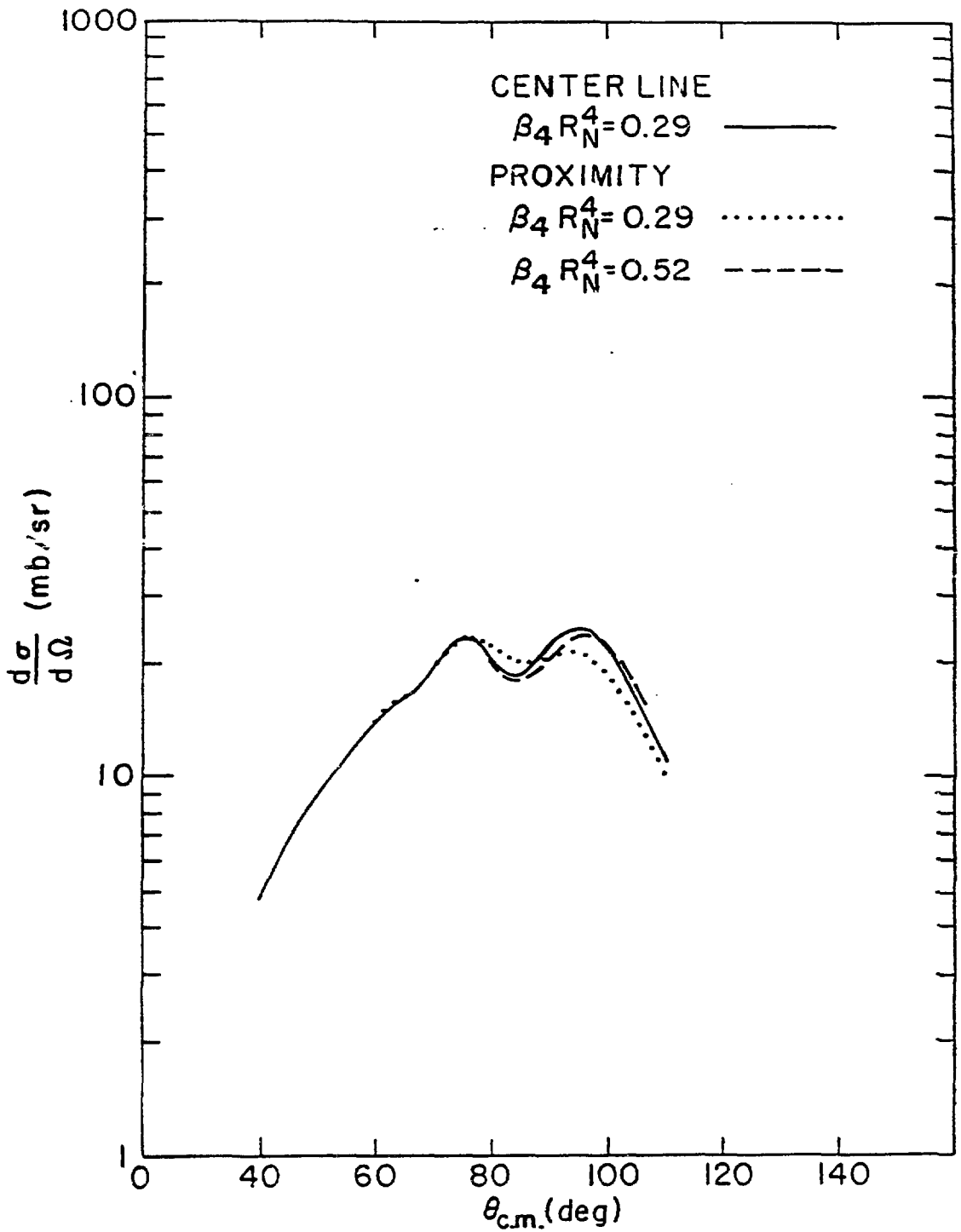


FIG. 3

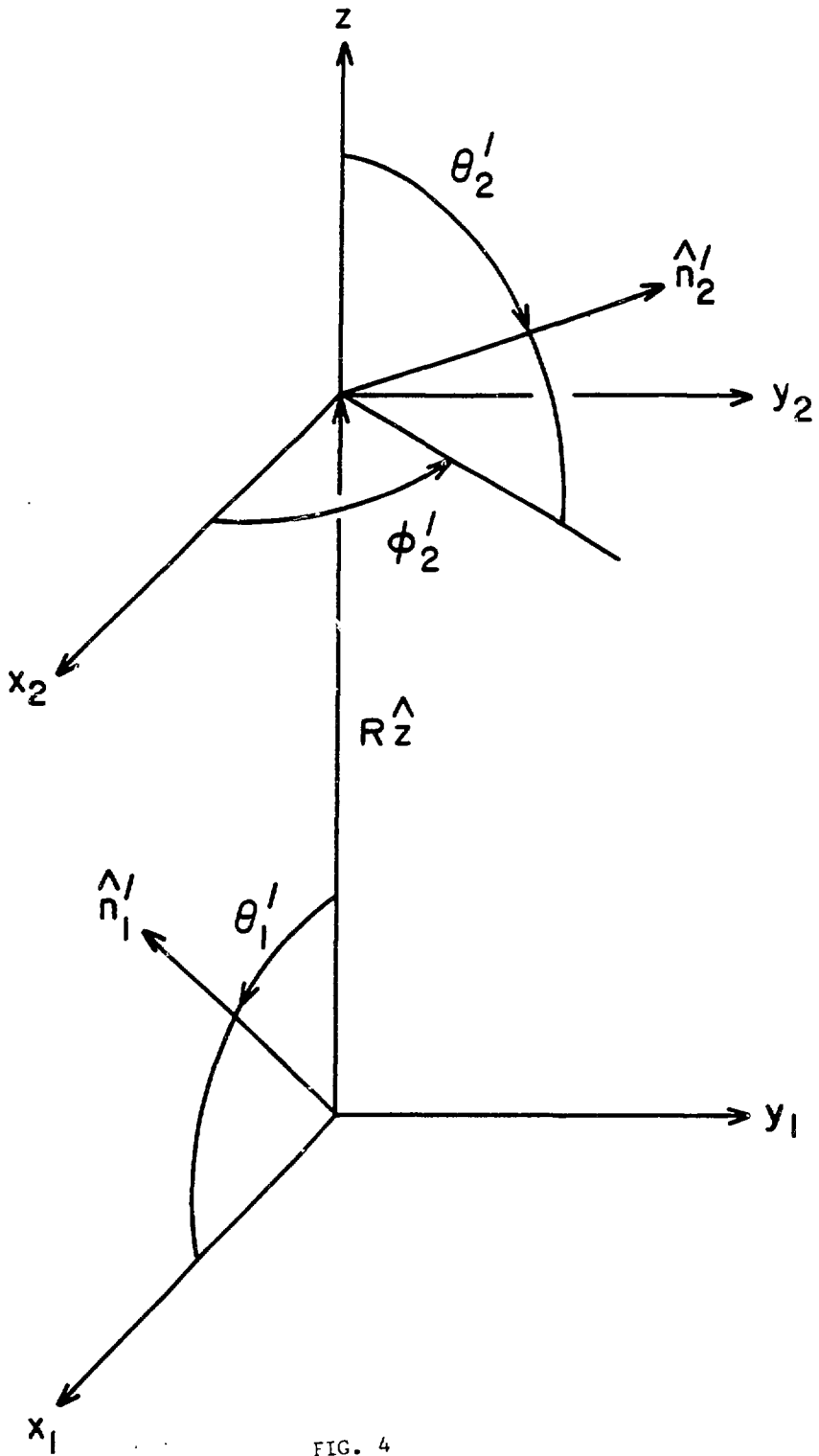


FIG. 4

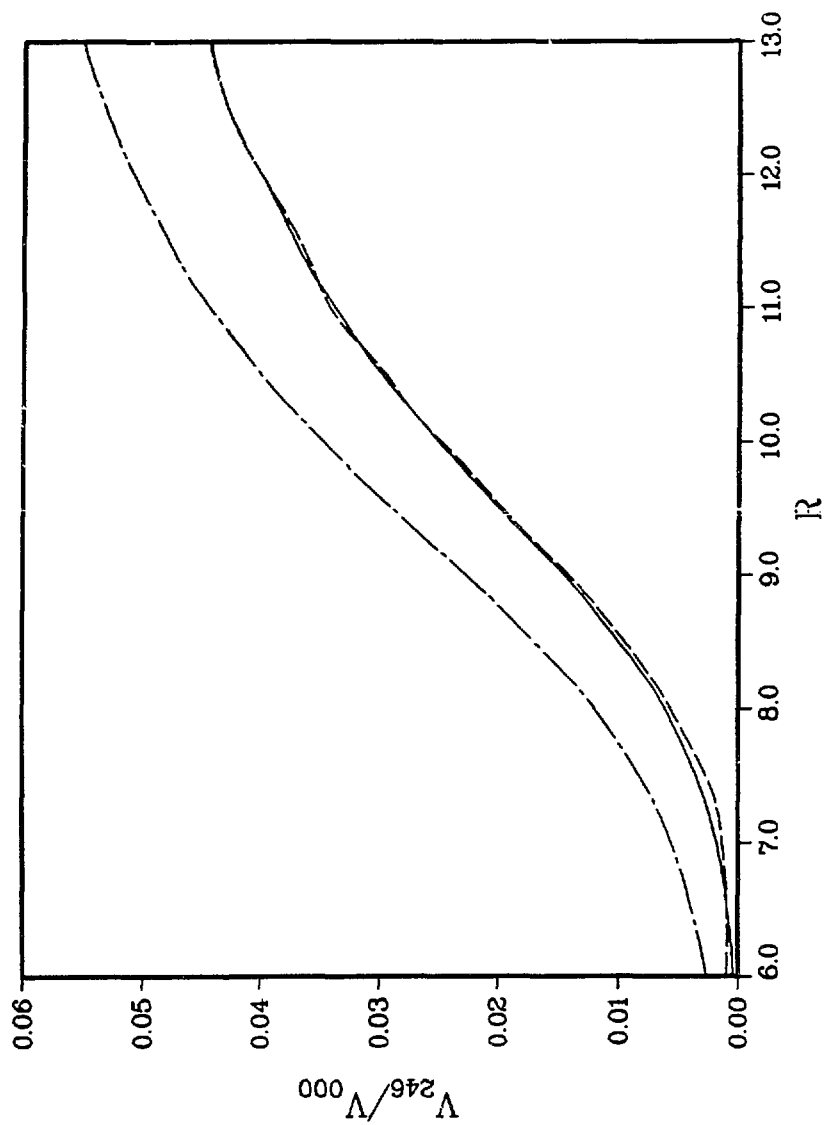


FIG. 5(a)

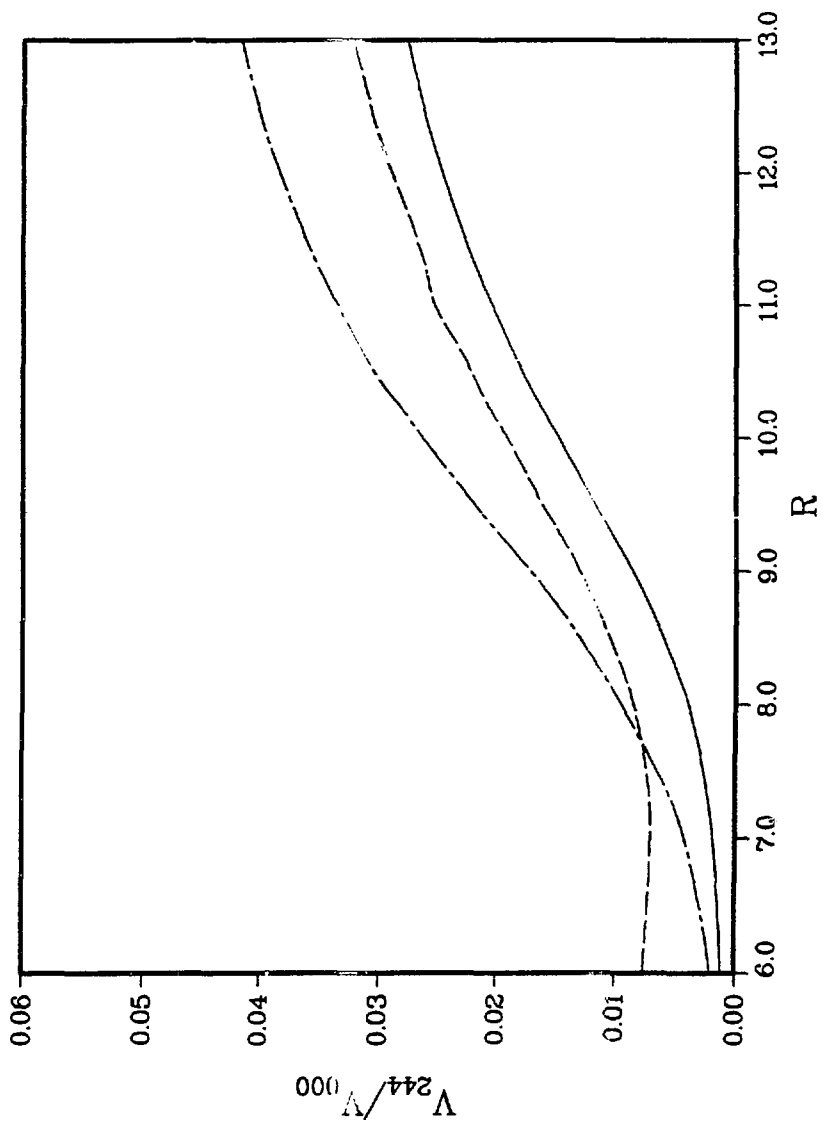


FIG. 5(b)

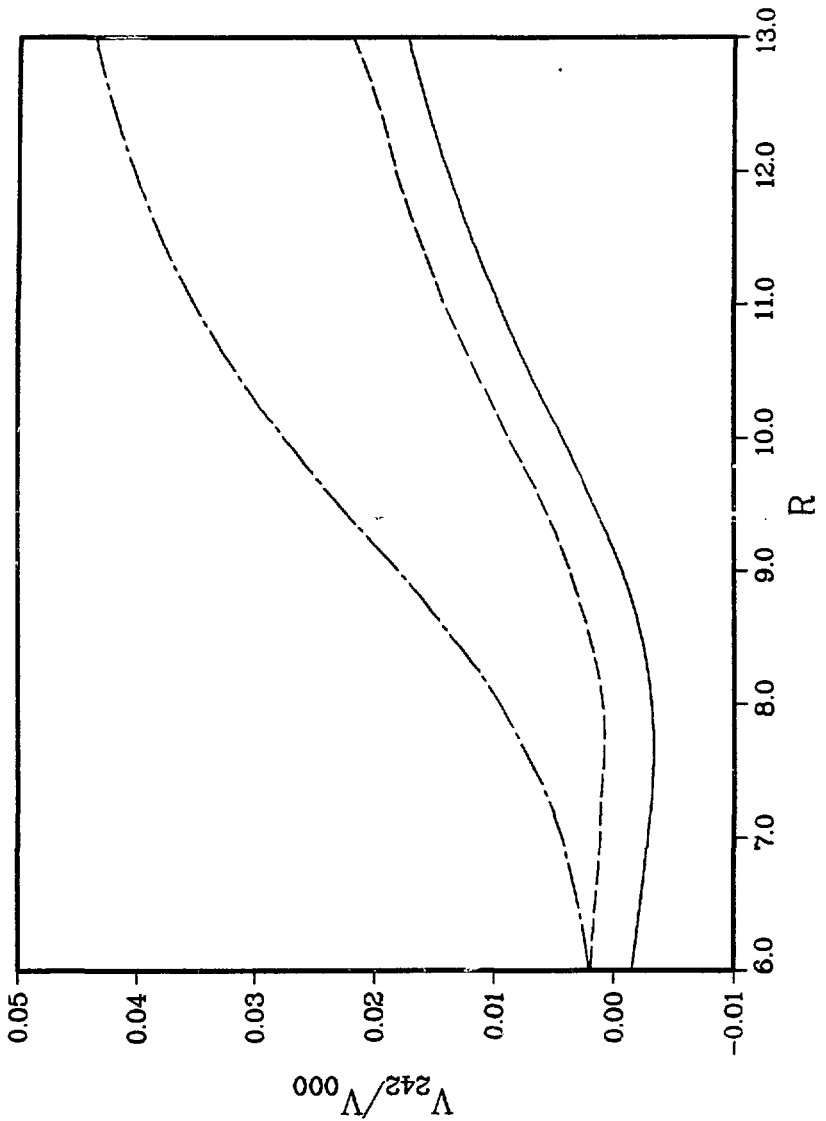


FIG. 5(c)

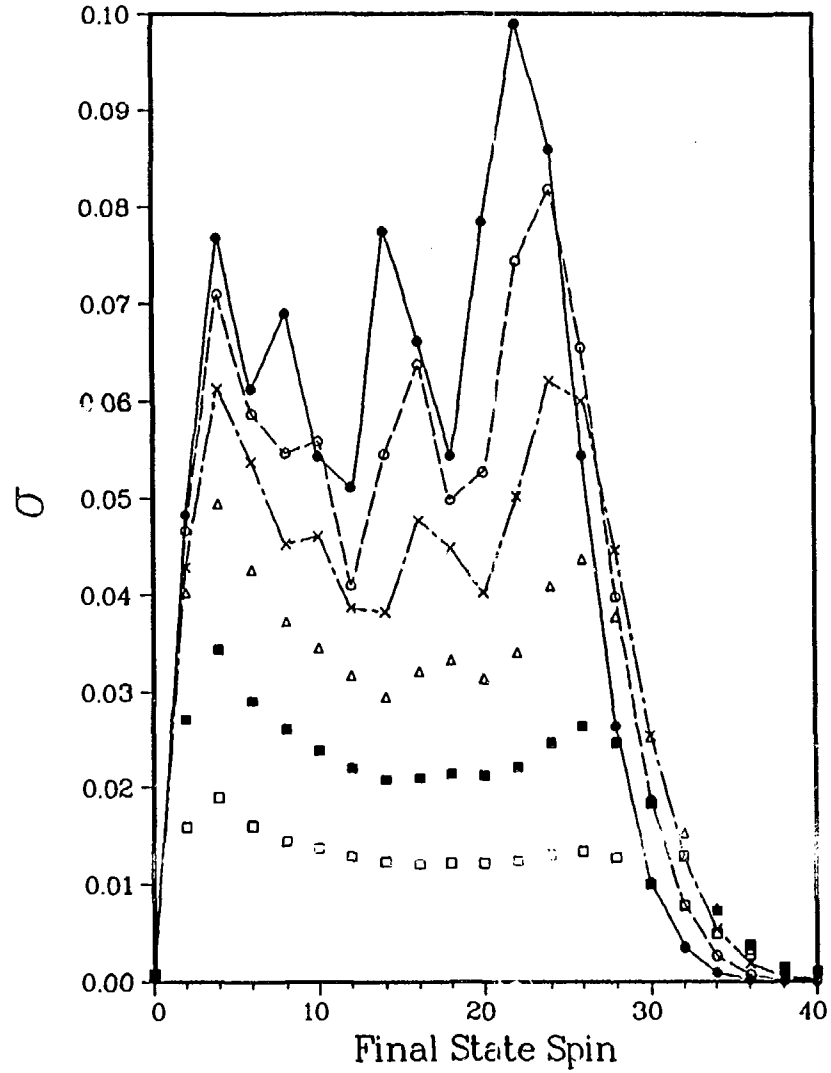


FIG. 6